Viscose-derived activated carbons fibers as highly efficient adsorbents for dimethoate removal from water
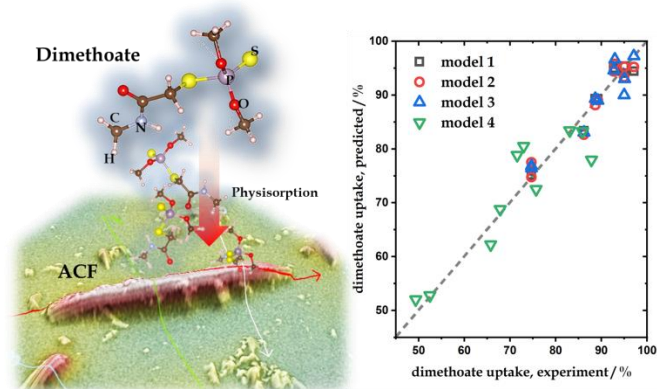
Ana Jocić[a], Stefan Breitenbach[b,c], Danica Bajuk-Bogdanović[d], Igor A. Pašti[d], Christoph Unterweger[b], Christian Fürst[b], Tamara Lazarević-Pašti[a]*

[a]University of Belgrade, VINČA Institute of Nuclear Sciences - National Institute of the Republic of Serbia, Mike Petrovica Alasa 12-14, 11000 Belgrade, Serbia.

[b]Wood K plus - Kompetenzzentrum Holz GmbH, Altenberger Strasse 69, 4040 Linz, Austria

[c]Institute of Chemical Technology of Inorganic Materials (TIM), Johannes Kepler University Linz, Altenberger Strasse 69, 4040 Linz, Austria

[d]University of Belgrade – Faculty of Physical Chemistry, Studentski trg 12-16, 11158 Belgrade, Serbia

*Corresponding author: lazarevictlj@yahoo.com, tamara@vin.bg.ac.rs

15   **Abstract**

16   Extensive use of pesticides resulting in their accumulation in the environment

17   presents a hazard for their non-target species, including humans. Hence, efficient

18   remediation strategies are needed, and adsorption is seen as the most

19   straightforward approach in this sense. We have studied activated carbon fibers

20   (ACFs) derived from viscose fibers impregnated with diammonium hydrogen

21   phosphate (DAHP). By changing the amount of DAHP in the impregnation step, the

22   chemical composition and textural properties of ACFs are effectively tuned, affecting

23   their performance for dimethoate removal from water. The prepared ACFs

24   effectively reduced the toxicity of treated water samples, both deionized water

25   solutions and spiked tap water samples, under batch conditions and in dynamic

26   filtration experiments. Using the results of physicochemical characterization and

27   dimethoate adsorption measurements, multiple linear regression models were made

28   to predict performance towards dimethoate removal from water reliably. These

29   models can be used to quickly screen among larger sets of possible adsorbents and

30   guide the development of novel, highly efficient adsorbents for dimethoate removal

31   from water.

32

33   **Keywords:** water remediation; dimethoate removal; activated carbon fibers;

34

1. Introduction

Pesticides are widely used to improve agricultural production and control various pests and disease vectors in public health. However, despite their many benefits, excessive or improper application of pesticides in agricultural activity leads to the pollution of soils and aqueous environments, which may produce a range of hazardous effects to non-target species such as humans and animals (Mojiri et al., 2020).

Organophosphorus pesticides (OPs) are among the most commonly used compounds to control pests for both agricultural and residential applications. Their usage is still growing because of their high efficacy, a broad spectrum of activity, multi-pest control capability, lack of pest resistance, and low cost (Wanjeri et al., 2018). However, the increased application of OPs leads to the pollution of land and water ecosystems and is a serious threat to human health due to the toxic nature of these compounds (Wanjeri et al., 2018). Their primary toxicity is associated with the irreversible inhibition of acetylcholinesterase enzyme (AChE) in the nervous system and blood, resulting in acetylcholine accumulation and consequently disrupted neurotransmission (Colovic et al., 2013).

Dimethoate (*O,O*-Dimethyl *S*-[2-(methylamino)-2-oxoethyl] phosphorodithioate) is an organophosphate used as a very effective insecticide and acaricide both in agriculture (the control of crop pests in soil and on foliage) and non-agricultural applications (the control of mosquitoes, flies, cockroaches, termite) (Ishag et al., 2016). According to the WHO classification, dimethoate belongs to second-class pesticides, which possess moderate toxicity (WHO, 2020). However,

58   their metabolites are a secondary pollution problem under optimum environmental

59   conditions and the influence of microbes, chemical or physical agencies. Dimethoate

60   tends to convert to much more toxic products than the primary pesticide (Colovic et

61   al., 2013). In specific, dimethoate can be readily transformed into its corresponding

62   oxo-form, omethoate, during drinking water disinfection processes (Tian et al.,

63   2014). In general, OP oxo-forms are more potent AChE inhibitors than their parent

64   pesticides (Colovic et al., 2013), which also holds for omethoate. Due to potentially

65   dangerous effects on human health, WHO has set a guideline value of 6 µg dm^{-3} for

66   dimethoate in water (WHO, 2017). Due to the high toxicity and tremendous effect of

67   OPs on the ecosystem, developing effective and economically feasible methods for

68   their removal from the environment is a global issue.

69   Different methods have been reported for OPs remediation, such as

70   bioremediation (Chishti et al., 2013; Ishag et al., 2016), photodegradation (Chen et al.,

71   2007; Farner Budarz et al., 2019; Samy et al., 2020), membrane filtration (Ahmad et

72   al., 2008) and adsorption techniques (Jacob et al., 2020; Lazarević-Pašti et al., 2016;

73   Liu et al., 2018; Momić et al., 2016). Among the mentioned methods, adsorption has

74   been considered one of the most suitable techniques for OP removal from an

75   aqueous medium due to its simplicity, cost effectiveness, environment friendliness,

76   and the possibility of scaling up the process (Liu et al., 2018).

77   Activated carbon fibers (ACFs) are suitable for contaminant adsorption

78   because of their unique and well-developed structural properties. They have a high

79   specific surface area (reaching up to 3000 m^2 g^{-1}) and uniform microporosity

80   (Breitenbach et al., 2020). Also, they can possess various surface functional groups

81 with an affinity for different adsorbates, so these features provide them high

82 adsorption kinetics and capacities (Hassan et al., 2020). Previous studies have

83 proved the ability of ACF to remove numerous pollutants contained in water,

84 namely pesticides (Faur et al., 2005), metal ions (Berber-Mendoza et al., 2018), and

85 organic micropollutants (Zhao et al., 2020). Moreover, studies have shown that the

86 adsorption capacity of pesticides by ACF is significantly higher than that of granular

87 activated carbon due to a smaller diameter of fibers which leads to a larger surface

88 area accessible to pesticides as well as narrower micropore size distribution which

89 enables a smaller mass transfer resistance (Cougnaud et al., 2005; Martin-Gullon and

90 Font, 2001). The structural and chemical characteristics and consequently adsorption

91 properties of the ACF mainly depend on the used precursor and the applied

92 production methods. Therefore, it is of great importance to find suitable raw

93 materials that contain favorable characteristics and, at the same time, are

94 economically and ecologically attractive. In this context, viscose fibers are

95 appropriate precursors for ACF preparation due to their fibrous structure, good

96 processability, bio-based origin, and availability with good and constant quality.

97 Moreover, using impregnation agents during the preparation of viscose-based ACFs

98 can significantly enhance the structural characteristics of the produced material and

99 reduce production costs by increasing yields (Breitenbach et al., 2020).

100 In this contribution, ACFs were prepared from viscose fibers impregnated

101 using diammonium hydrogen phosphate (DAHP). Using DAHP in a wide

102 concentration range, chemical composition and textural properties of produced

103 ACFs were effectively tuned, while fibrous morphology was preserved. Produced

104 ACFs were used as adsorbents for dimethoate in water and displayed high efficiency

105 for its removal under both batch and dynamic conditions. Materials performance

106 and guidelines for developing novel materials for dimethoate removal are discussed

107 in terms of their physicochemical properties.

108

109 **2. Material and methods**

110 2.1. Materials synthesis

111 In the first step, viscose fibers (1.7 dtex, 38 mm) were dried for 24 h at 90 °C

112 and then impregnated for 15 min in different solutions of DAHP in deionized water.

113 The concentrations ranged from 0.0–75.7 mmol dm^{-3}, matching 0.0–10.0% DAHP in

114 distilled water. Upon impregnation, fibers were spin-dried for 15 min and then

115 stored in a drying cabinet at 90 °C for 24 h. Next, carbonization was done in a

116 chamber furnace (HTK8, Gero, Germany) under a nitrogen atmosphere. The heating

117 rate was 1.0 °C $min^{-1,}$ and upon reaching 850 °C they were held isothermal for 20

118 min. Finally, the carbonized fibers were activated in a rotary kiln at 870 °C for 165

119 min in a CO_2-flow of 80 dm^3 h^{-1}. The samples are noted as DAHP-X, where X stands

120 for the concentration of DAHP used in the impregnation step.

121

122 2.2. Materials characterization

123 The morphology of the ACF samples was investigated using a scanning

124 electron microscope Phenom ProX (Thermo Fisher Scientific, USA).

125 The specific surface area and textural structures of the obtained ACFs were

126 analyzed by N_2 isothermal adsorption (−196.15 °C) on a gas sorption system

127   (Autosorb iQ, Quantachrome Instruments, USA). The samples were de-gassed for at

128   least 2 h at 200 °C before the analysis. The specific surface area and derived pore size

129   distribution (PSD) were calculated using the method of Brunauer-Emmett-Teller

130   (BET) and the non-local density functional theory (NLDFT), respectively.

131   The Raman spectra of the samples were recorded on DXR Raman microscope

132   (Thermo Fisher Scientific, USA). The samples were excited by the 532 nm emission

133   line of a diode laser with 2 and 8 mW of power focused on a 2.1 µm spot on the

134   surface of the sample. The spectrum was obtained as an average of three

135   measurements on different spots on each sample (10 exposures, 10 s each, per place).

136   The FTIR spectra were recorded on a Nicolet iS20 FT-IR spectrophotometer

137   (Thermo Fisher Scientific, USA) using the KBr pellet technique in a wavenumber

138   range from 4000 to 500 cm^{-1} with 64 scans and 4 cm^{-1} resolution. All FTIR spectra are

139   shown after automated baseline correction (polynomial order: 2, number of

140   iterations: 20) performed by OMNIC software (Thermo Fisher Scientific, USA).

141

142   2.3. Pesticide adsorption measurements

143   Batch adsorption experiments were done as follows. First, prepared ACFs

144   were dispersed in double distilled water, upon which the desired amount of

145   dimethoate stock solution (Pestanal, Sigma Aldrich, Denmark) was added to provide

146   the targeted concentration of adsorbent and dimethoate. Then, the vessel containing

147   the adsorbent+dimethoate mixture was placed on a laboratory shaker (Orbital

148   Shaker-Incubator ES-20, Grant-Bio, UK) at 25 °C for desired times. Afterwards, the

149   mixture was centrifuged for 10 min at 14500 rpm, and the supernatant was filtered

150 through the nylon filter (pore size 220 nm KX Syringe Filter, Kinesis, UK). The

151 concentration of dimethoate after adsorption (C_{eq}) was determined using Ultra

152 Performance Liquid Chromatography (UPLC). Control experiments were performed

153 in identical ways but without ACFs and confirmed no dimethoate degradation

154 during the batch experiments.

155   To perform adsorption measurements under dynamic conditions, commercial

156 nylon membrane filters (pore size 220 nm KX Syringe Filter, Kinesis, UK) were

157 modified to include the adsorbent layer, as described in ref. (Lazarević-Pašti et al.,

158 2016). The desired amount of each ACF sample was dispersed in 1.5 cm^3 of

159 deionized water and injected into the commercial filter. Then, the solvent was

160 removed from the ACFs-modified filter using compressed air. Pesticide solution was

161 run through the modified filter for 1 min. The filtrate was subjected to UPLC

162 analysis to determine the concentration of pesticide after filtering. It was checked

163 that dimethoate removal is not due to the nylon membrane by comparing pesticide

164 concentrations before and after the filtration through the non-modified filter. The

165 efficiency of a modified filter towards dimethoate removal was also quantified as the

166 pesticide uptake.

167   For both sets of experiments, the efficiency of adsorption was measured by

168 dimethoate uptake calculated as Uptake = 100% × $(C_0 - C_{eq})/C_0$, where C_0 is the

169 starting concentration of dimethoate. It is important to note that we confirmed that

170 there is no decomposition of dimethoate under experimental conditions. Hence, the

171 reduction of dimethoate concentration is solely due to the adsorption by studied

172 ACFs.

173   For UPLC measurement, an ACQUITY UPLC system (Waters, USA) with a

174   tunable UV detector, controlled by the Empower software, was used. The analyses

175   were done using an ACQUITY UPLC™ BEH C18 column (1.7 µm, 100 mm × 2.1 mm,

176   Waters, USA) under isocratic conditions with a mobile phase consisting of 10%

177   acetonitrile and 90% water (v/v). The eluent flow rate was 0.2 cm³ min⁻¹, and the

178   injection volume was 10 mm³. Under these experimental conditions, the retention

179   time of dimethoate was 2.6 min. Dimethoate was detected at 200 nm.

180

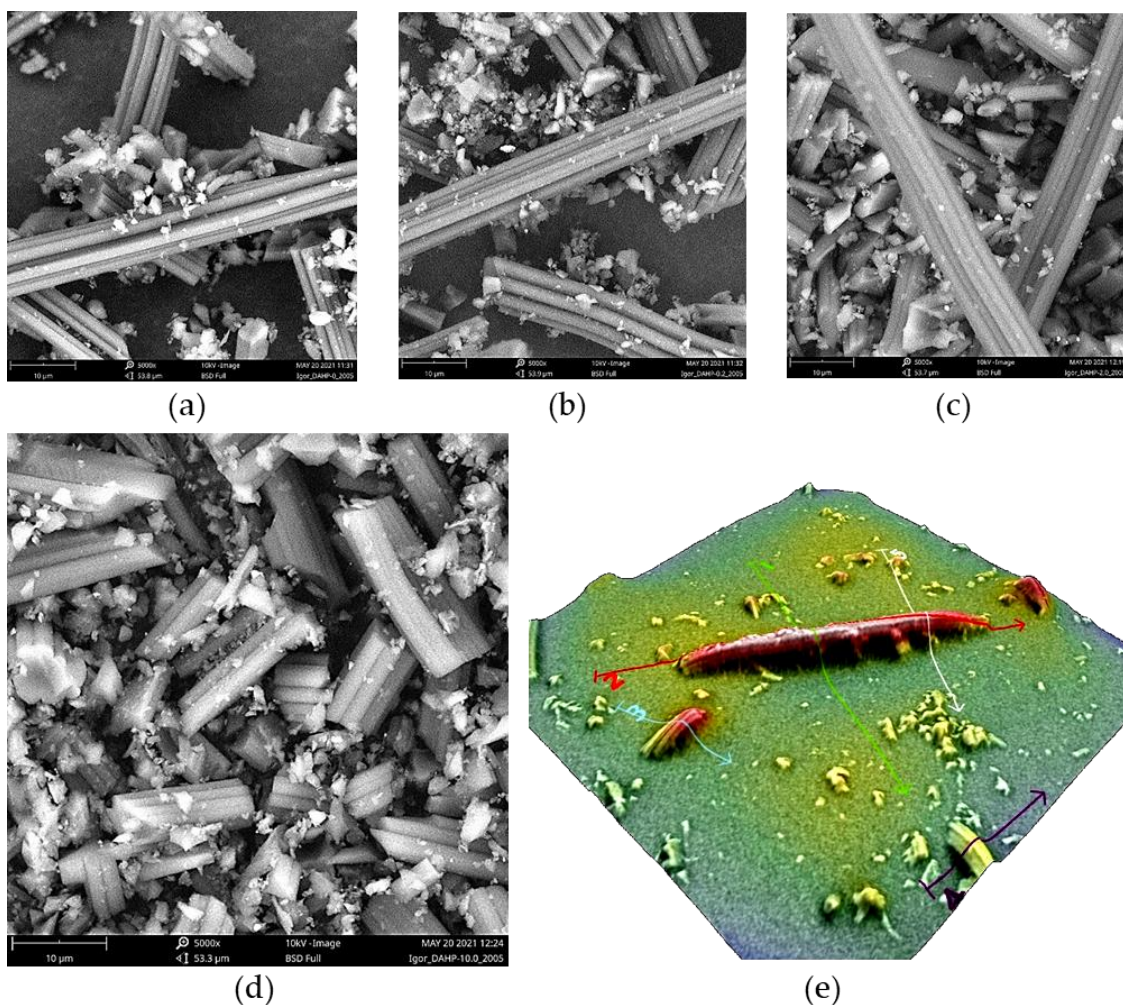181   2.4. Toxicity testing

182   AChE activity was assayed according to modified Ellman's procedure (Ellman

183   et al., 1961). Briefly, the *in vitro* experiments were performed by exposing 2.5 IU of

184   commercially purified AChE from electric eel to treated OP solutions obtained in

185   adsorption experiments (filtered supernatants in batch experiments, or filtrates in

186   dynamic adsorption experiments) at 37 °C in 50 mM PB pH 8.0 (final volume

187   0.650 cm³). The enzymatic reaction was started by adding acetylcholine-iodide in

188   combination with 5,5′-Dithiobis(2-nitrobenzoic acid) (DTNB) as a chromogenic

189   reagent and proceeded to proceed for 8 min. Then, it was stopped by adding 10%

190   sodium dodecyl sulfate. Thiocholine, which is the enzymatic reaction product, reacts

191   with DTNB and forms 5-thio-2-nitrobenzoate, whose absorbance was measured at

192   412 nm. AChE concentration was kept constant in all experiments and previously

193   optimized to give an optimal spectrophotometric signal. The toxicity of treated water

194   samples was quantified *via* the AChE inhibition given as

195   AChE inhibition (%) = 100% × (A_0 − A) / A, where A_0 and A stand for the AChE

196   activity in the absence of OP (control) and the one measured after the exposure to a

197   dimethoate solution, respectively.

198

199   **3. Results and discussion**

200   3.1. Materials morphology and chemical composition using EDX

201   Using SEM, we have found that the morphology of all prepared ACF samples

202   is the same and reflects, besides a shrinkage of approx. 30%, the morphology of

203   precursor viscose fibers, in agreement with our previous findings (Breitenbach et al.,

204   2021). SEM micrographs are presented in **Figure 1**. Certain ACFs broke into smaller

205   pieces during the milling step, while some intact ACFs are also seen, with lengths

206   reaching 200 μm and approx. 8 μm in diameter (**Figure 1e**).

207
208 **Figure 1.** SEM micrographs of (a) DAHP-0, (b) DAHP-0.2, (c) DAHP-5.0, (d) DAHP-
209 10, and (e) 3D reconstruction of individual small fiber debris showing diameter of
210 ACFs of roughly 8 μm.
211

212 In contrast to morphology, the chemical composition of ACFs was affected by the

213 loading of DAHP during the impregnation. Using EDX, we observed an increased P

214 content in ACFs, as summarized in Table 1. The results follow the trend reported

215 previously for ACFs produced from DAHP-impregnated viscose fibers, but O

216 content is significantly larger (Breitenbach et al., 2020). This might be due to the

217 adhesive tape used to paste the powders onto the SEM holder, which contains a

218 large fraction of O (and additional C), but this effect produces a constant bias in

219 oxygen content determined in the samples.

220

Table 1. Elemental composition of studied ACFs obtained using EDX. Presented results are averaged over four individual spot measurements.

	Carbon		Oxygen		Phosphorus	
DAHP-X	at.%	Δ(at.%)	at.%	Δ(at.%)	at.%	Δ(at.%)
0	92.4	2.1	7.6	2.0	0	-
0.25	91.6	3.5	8.4	3.5	0.02	0.02
0.5	93.6	2.3	6.2	2.2	0.18	0.10
1	87.9	1.3	12.0	1.3	0.11	0.04
1.5	93.9	1.9	5.9	1.9	0.28	0.07
2	91.3	2.0	7.7	2.3	0.91	0.29
2.5	87.9	2.0	11.4	2.2	0.65	0.30
5	85.6	2.5	13.1	2.7	1.32	0.34
7.5	82.2	2.2	16.1	2.3	1.78	0.13
10	77.8	5.0	19.7	5.3	1.90	0.64

223

It is important to note that the distributions of C, O, and P were rather uniform in the samples, as seen from the EDX mapping under low magnification and mapping on individual fibers (**Figure 2**). We also found that P incorporation is not observed only on the surface but also in the inner part of ACFs, as EDX confirmed the presence of P along the cross-section of ACFs (**Figure 3**). This indicates that DAHP entered the pores of precursor viscose fibers during the impregnation step and resulted in the incorporation of P throughout the entire volume of ACFs.
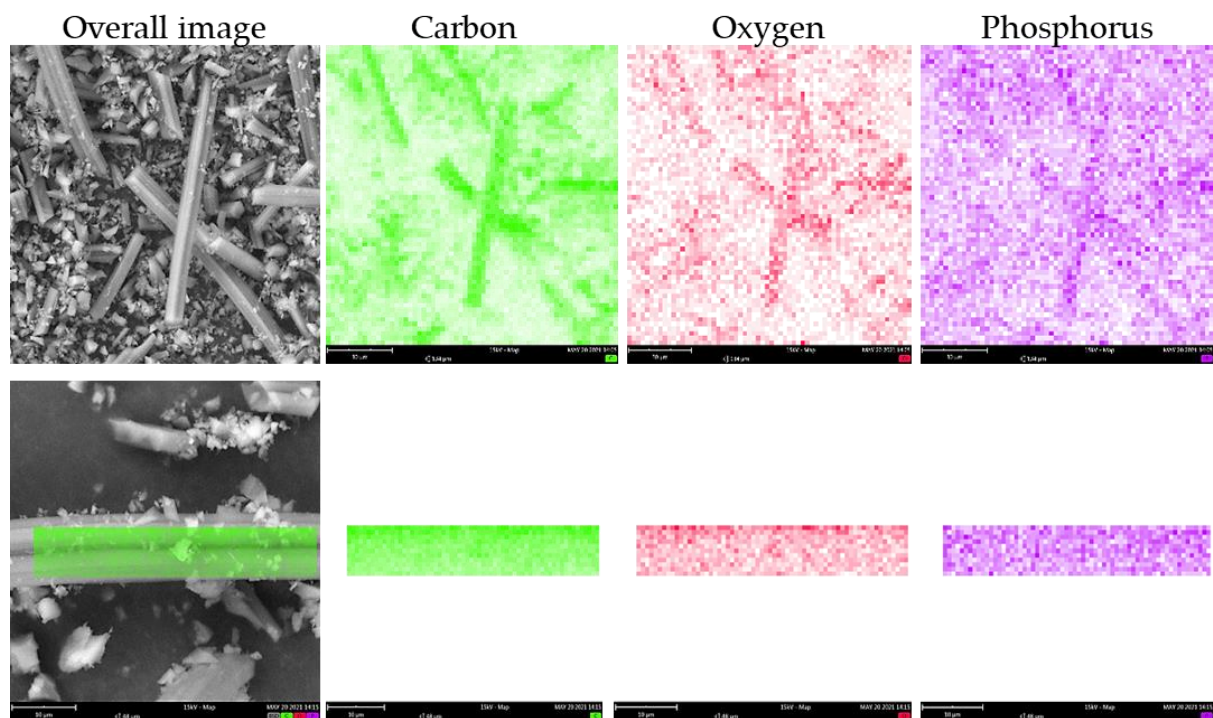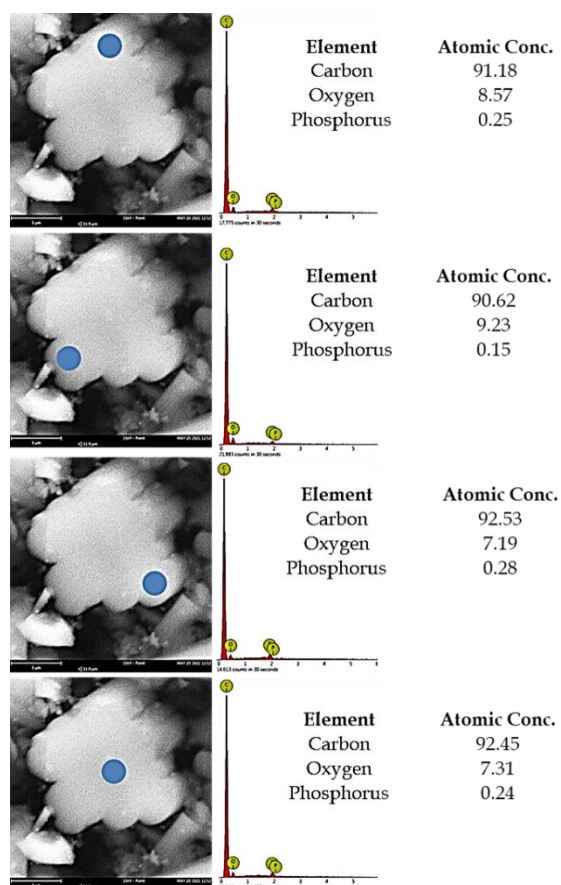
231

Figure 2. EDX mapping for sample DAHP-2.5

Figure 3. EDX analysis along the cross-section of the DAHP-2.5 sample

13

237

3.2. Textural properties
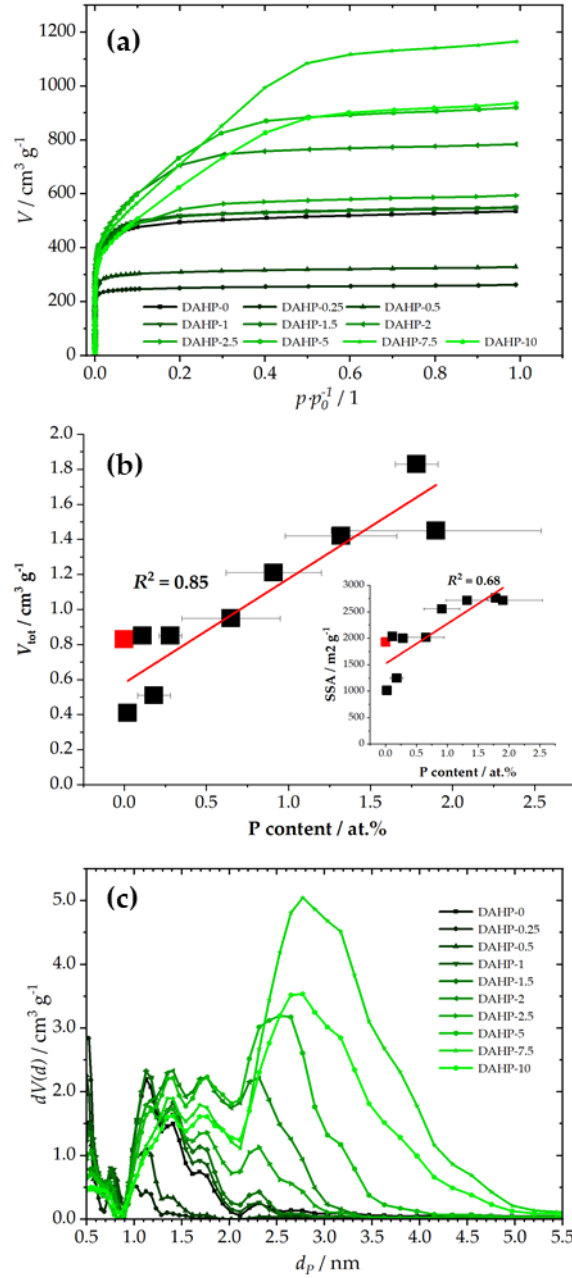
The specific surface area (SSA) and total pore volume (V_{tot}) for each sample

determined using N_2 adsorption measurements (**Figure 4a**) are shown in **Table 2**.

241

Table 2. Specific surface areas (SSA) and total pore volumes (V_{tot}) of studied
samples.

DAHP-X	SSA / m² g⁻¹	V_{tot} / cm³ g⁻¹
0*	1932	0.83
0.25	1016	0.41
0.5*	1250	0.51
1	2037	0.85
1.5*	2002	0.85
2	2556	1.21
2.5*	2018	0.95
5*	2718	1.42
7. 5	2763	1.83
10	2718	1.45

*ref (Breitenbach et al., 2020)

245

The first P-containing sample in the series showed a large decrease in SSA compared

to the ACFs produced without DAHP impregnation. However, upon increasing the

DAHP concentration SSA and V_{tot} increase. One can consider that the sample

DAHP-2 is an outlier, but according to the EDX results, this sample also contains a

larger fraction of P incorporated in the structure. Thus, there is a rather good

correlation between V_{tot} and SSA, on one side, and P content on the other (**Figure 4**,

middle).

253

Figure 4. Adsorption isotherms (a), the correlation between V_{tot} and P content (inset gives the correlation between SSA and P content; lines give linear fit; red square stands for DAHP-0 sample) and derived PSDs (b) for the studied samples.
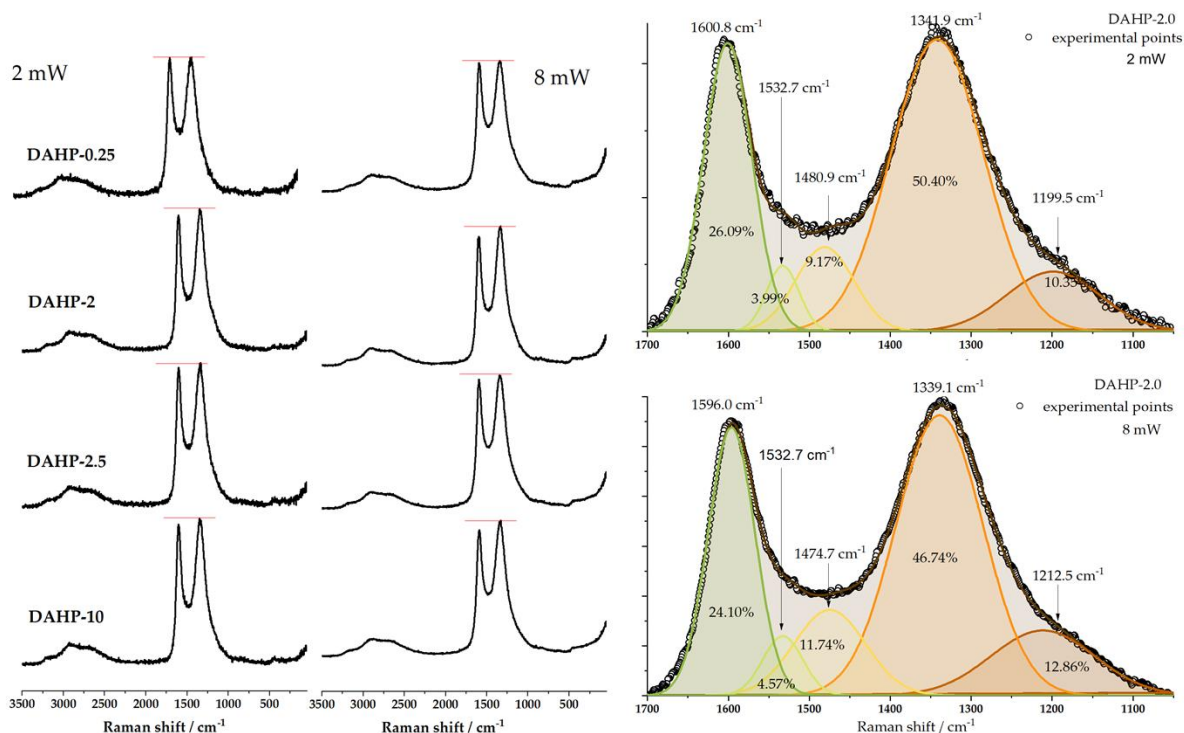
This correlation is very important when it comes to the impact of different properties of studied materials on the adsorption performance, as will be discussed further. In addition, we also note that SSA and V_{tot} are in excellent correlation, although at the high SSA side, this correlation deviates from a straight line. This is

263   because the increase of the P content causes the shift of the dominant pore range

264   from microporous to mesoporous (**Figure 4b**). Hence, the increase of P content (and

265   O content simultaneously) results in a gradual increase in pore sizes.

266

267   3.3. Raman and FTIR spectroscopy
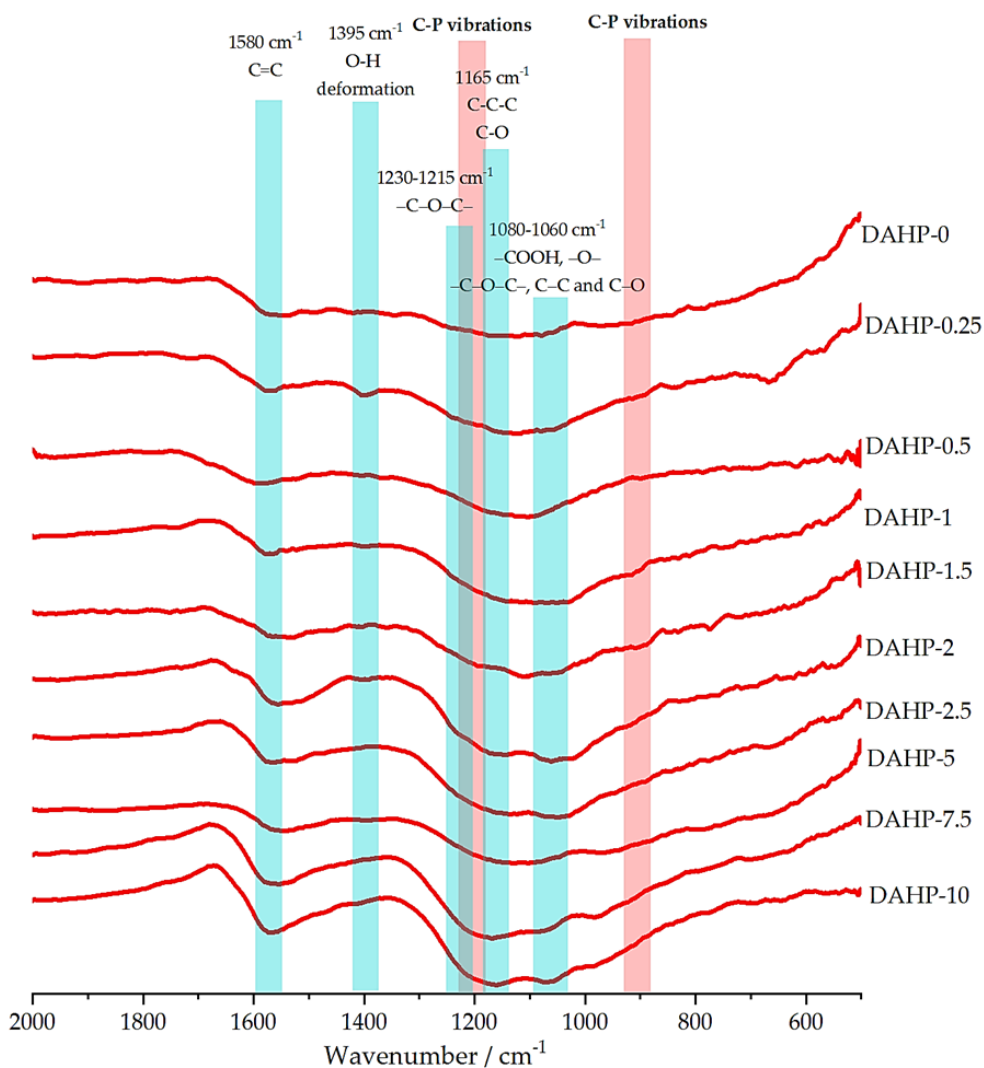
268   Since Raman spectroscopy is one of the most frequently used techniques to

269   investigate carbon materials, the spectra were recorded for the studied samples

270   (**Figure 5**). Interestingly, despite the different chemical compositions of the samples,

271   we could not differentiate between the recorded spectra in such a way as to outline

272   any particular trend. However, characteristic bands around 1340 and 1580 cm^{-1} are

273   clearly seen. These are assigned to D (originating from sp^3-hybridized carbon) and G

274   band (originating from the sp^2-hybridized graphitic phase of the carbon) (Ferrari and

275   Robertson, 2000). The change of the laser power from 2 to 8 mW only slightly

276   affected the D and G band intensities ratio but did not manage to differentiate

277   between the studied samples to an appreciable level. Taking the sample DAHP-2.0

278   as an example, the Raman signal of D and G band regions can be split into five

279   components (Ferrari and Robertson, 2000; Shimodaira and Masui, 2002), and if the

280   peak areas are used to evaluate the I_D/I_G ratio, the result is 1.93 for 2 mW and 1.94

281   mW for 8 mW laser power. However, the numbers themselves indicate the presence

282   of a significant number of defects in the ACFs structure.

Figure 5. Representative Raman spectra of prepared ACFs with two different laser powers (2 mW, left column, and 8 mW, right column). Horizontal bars are included for easier comparison of D and G bands intensities. On the right, deconvolution of Raman spectra of DAHP-2.0 sample is presented for the laser power of 2 and 8 mW. Positions of individual bands and their relative contributions to the overall signal in the considered wavenumber range are indicated.

FTIR spectra (**Figure 6**) showed a clear evolution with increasing P content. The assignation was done according to (Shanmuga Priya et al., 2020; Țucureanu et al., 2016), suggesting that with the increase of the P content, bands associated with C=C vibrations (1580 cm^{-1}) and particularly vibrations of O containing groups (–C–O–C–, –COOH, –O–, C–O, and others), in the range between 1250 and 1000 cm^{-1} become more pronounced. Moreover, the bands of the mentioned O containing groups also fall in the range of wavenumbers at which the vibrations of the C–P moieties can be found (around 1200 cm^{-1}, while the C–P can also appear around 900 cm^{-1}) in organic P-containing molecules (Thomas and Chittenden, 1965).
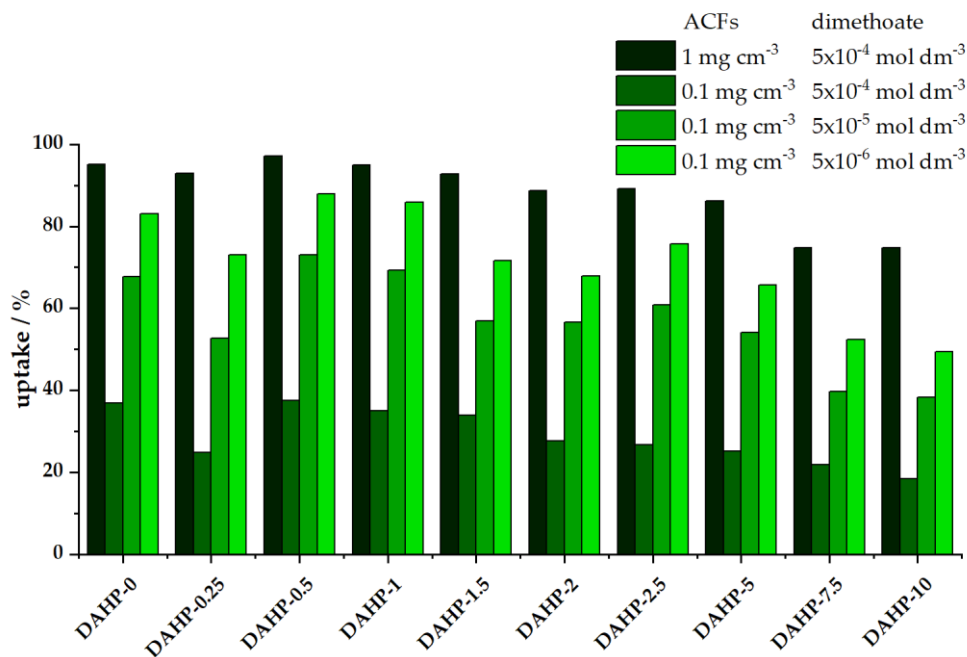
17

Figure 6. FTIR spectra (transmittance) of the investigated samples with bands assignation. At higher wavenumbers, only characteristic OH vibration at 3400 cm^{-1} is seen in all samples. The ranges where the C-P vibrations are found are also indicated.

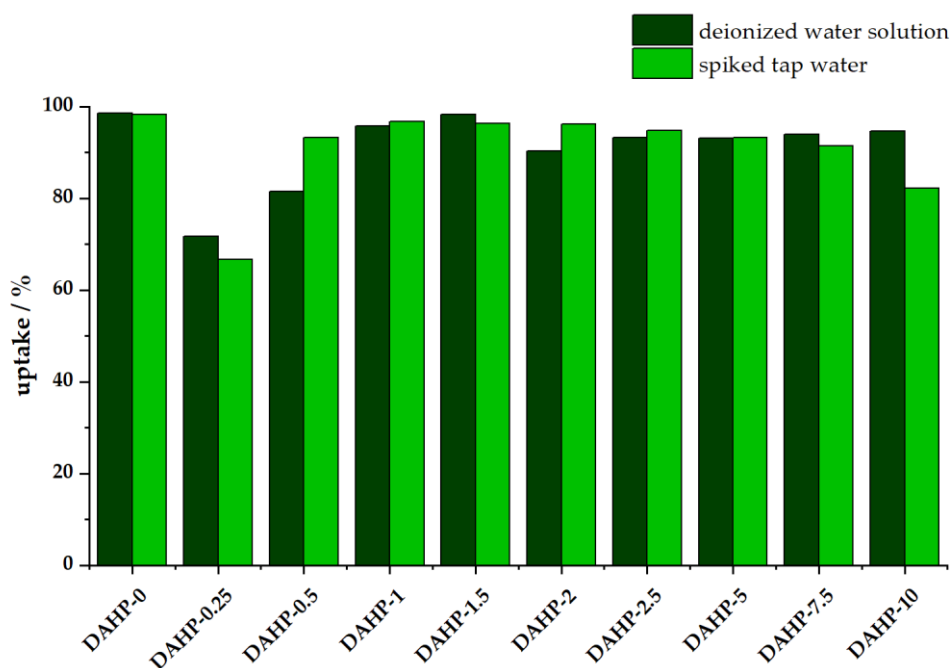3.4. Dimethoate removal from aqueous solutions

Following the physicochemical characterization of the ACFs, we studied dimethoate removal under bath (equilibrium) conditions and under dynamic conditions (filtration). Preliminary experiments showed that 20 min of equilibration time is sufficient to reach steady conditions. The results for the adsorbent concentration of 1 mg cm^{-3} and dimethoate concentration of 5×10^{-4} mol dm^{-3} are

18

312   shown in **Figure 7**. We also tested dimethoate removal for a lower concentration of

313   ACFs (0.1 mg cm^{-3} and different concentrations of dimethoate (5×10^{-4} mol dm^{-3},

314   5×10^{-5} mol dm^{-3}, and 5×10^{-6} mol dm^{-3}), **Figure 7**. We observe that the trends are

315   preserved in all the cases: the best performance is seen for materials with low P

316   content, reaching maximum for the DAHP-0.5 sample, taking 97 % of dimethoate

317   from the 5×10^{-4} mol dm^{-3} solution (ACFs concentration 1.0 mg cm^{-3}). Upon

318   increasing the P content, dimethoate uptake decreases and falls below 80% for the

319   DAHP-7.5 and DAHP-10 samples. As these samples have the highest SSAs of all the

320   studied ACFs, this is a very clear indication that SSA solely does not determine the

321   performance of dimethoate removal from water under equilibrium conditions.

322   Nevertheless, these materials are not bad dimethoate adsorbents but perform much

323   lower than the other ACFs in the studied series. When the amount of adsorbed

324   dimethoate is expressed as the adsorption capacity, giving the mass of dimethoate

325   adsorbed *per* unit mass of ACFs, these values range between 111 and 86 mg g^{-1}

326   (experiments done using 1 mg cm^{-3} of ACFs and dimethoate concentration of 5×10^{-4}

327   mol dm^{-3}). It is important to note that the better performance of ACFs impregnated

328   with lower concentrations of DAHP is also very beneficial from a practical point.

329   Namely, the total yield of ACFs after carbonization and activation steps is

330   maximized for low concentrations of DAHP as an impregnation agent (reaching

331   20%, (Breitenbach et al., 2020). The yield is much higher than the yield when no

332   DAHP is used (~1%) and when high concentrations of DAHP are used (yields

333   ranging 6-10%).

334

Figure 7. Dimethoate removal (in %) under batch conditions for different concentrations of ACFs and dimethoate (20 min equilibration time, 25 °C).

Under dynamic conditions, materials performed similarly in deionized and spiked tap water samples, suggesting that matrix effects are rather small (**Figure 8**). In this case, the lowest performance was observed for the sample DAHP-0.25, which has the lowest SSA (**Table 2**). It is followed by DAHP-0.5 and DAHP-10 samples, while other samples have dimethoate uptake above 90% in both deionized water and spiked tap water solutions. However, the complexity of dimethoate removal under dynamic conditions is much higher compared to the equilibrium adsorption conditions, but the obtained results suggest, again, that SSA is not the dominant factor for dimethoate removal.

348

Figure 8. Dimethoate removal under dynamic conditions. Filters were filled with 1 mg of ACFs, and then 1 cm^{-3} of 5×10^{-4} mol dm^{-3} dimethoate solution was filtered for 1 min through them (25 °C).

As organophosphates are neurotoxic agents, it is important to verify the reduced toxicity of purified water samples. Another important point is that oxo-forms of organophosphate pesticides are even more toxic than their parental thio-forms, so one has to exclude the possibility of dimethoate oxidation during the water remediation process. This result is very important as we have recently shown that dimethoate can react with O-rich carbon using graphene oxide as an example (Anićijević et al., 2021). The experiments were done using spiked tap water samples, and an efficient reduction of water toxicity is clearly seen (**Table 3**). As higher AChE inhibition level correlates with lower dimethoate uptake, the toxicity measurements are in excellent correlation with the bath and filtration measurements. Under dynamic conditions, the most effective ACFs are DAHP-0, while under batch

21

364   conditions, DAHP-0.5 leads the series. Both samples completely alleviate any water

365   toxicity upon the treatment under mentioned conditions.

366

367   **Table 3.** AChE inhibition before and after adsorption; Filter: adsorbent 1 mg cm^{-3},
368   dimethoate 5×10^{-4} mol dm^{-3} in tap water, 1 min time of filtration, 25 °C; batch:
369   adsorbent 1 mg cm^{-3}, dimethoate 5×10^{-4} mol dm^{-3} in tap water, 20 min contact time
370   in batch, 25 °C

Adsorbent DAHP-X	AChE inhibition before adsorption (% of control)	AChE inhibition after adsorption in (% of control)	
		filter	batch
0	35	0	5
0.25	35	15	5
0.5	35	5	0
1	35	5	5
1.5	35	5	5
2	35	5	15
2.5	35	7	12
5	35	9	18
7.5	35	9	20
10	35	12	21

371

372   3.5. Adsorption isotherms for dimethoate removal

373   To better understand the adsorption of dimethoate onto studied ACFs, we

374   fitted our experimental data obtained under equilibrium conditions into several

375   frequently used adsorption isotherms. The equations of used isotherms and their

376   linearized forms are summarized in **Table 4**.

377

378   **Table 4.** The equations of used isotherms and their linearized forms

Isotherm	Equation	Linearized form
Freundlich	$q_{\mathrm{e}} = K_{\mathrm{f}} C_{\mathrm{e}}^{1/n}$	$\log q_e = \log K_f + \dfrac{1}{n} \log C_e$

22

Langmuir	$q_e = \dfrac{q_{max} b C_e}{1 + b C_e}$	$\dfrac{C_e}{q_e} = \dfrac{1}{b q_{max}} + \dfrac{C_e}{q_{max}}$
Dubinin-Radushkevich	$q_e = q_{DR} \exp(-K_{DR} \varepsilon^2)$	$\ln q_e = \ln q_{DR} - K_{DR} \varepsilon^2$

379 *ref (Al-ghouti and Da'ana, 2020)

380   In **Table 4,** the used parameters are: q_e (mg g^{-1}) equilibrium adsorption

381 capacity, C_e (mg dm^{-3}) equilibrium adsorbate concentration, K_f (mg g^{-1} (mg dm^{-3})$^{1/n}$)

382 and Freundlich constants, q_{max} (mg g^{-1}) theoretical maximum adsorption capacity of

383 the monolayer, b (dm^3 mg^{-1}) Langmuir constant, q_{DR} maximum adsorption capacity,

384 K_{DR} (mol^2 J^{-2}) constant associated with the mean free adsorption energy *per* mole of

385 adsorbent, E free adsorption energy per mole adsorbent $E = (-2K_{DR})^{-1/2}$, ε = RT ln (1

386 + $1/C_e$). We used linearized forms of isotherms to fit the experimental data and user

387 R^2 to measure the quality of the fit. The obtained results are summarized in **Table 5**.

388   According to Langmuir's model, dimethoate molecules should be adsorbed

389 on an energetically homogeneous surface, in a monolayer, without interactions

390 between the adsorbed molecules. All active centers are energy equivalent, and

391 equilibrium is achieved by forming a monolayer of adsorbents on the adsorbate

392 surface. Constant b has the highest value in the adsorption of dimethoate on DAHP-

393 0.5 (0.010 dm^3 mg^{-1}). Higher values of this constant indicate an increased affinity of

394 given ACFs towards dimethoate. However, the Langmuir model gives extremely high

395 values of the maximum adsorption capacity of the monolayer (q_{max} up to

396 4000 mg g^{-1}), which is not in accordance with the literature data for pesticide

397 adsorption on carbon materials. Therefore, despite high R^2 values, this model is not

398 suitable for describing experimental data.

399   Freundlich's model predicts adsorption on an energetically heterogeneous

400   surface, where the adsorbed molecules interact with each other. If $n = 1$, the

401   adsorption follows the linear function. If $n < 1$, the adsorption is unfavorable, and if

402   $n > 1$, the adsorption is favored. The values of n obtained by fit are all above 1, so the

403   affinity of dimethoate for the adsorbent is high and the highest for DAHP-0.5.

404   The Dubinin-Radushkevich (DR) model can explain the nature of the

405   adsorption process, that is, whether physisorption or chemisorption predominates

406   on the adsorbent surfaces. Namely, the free adsorption energy E can be calculated

407   from the DR equation, and if higher than 8 kJ mol^{-1}, chemisorption prevails in the

408   system, while lower values indicate physisorption. In the tested systems, the

409   obtained E values are significantly lower than 8 kJ mol^{-1}. Therefore, it can be

410   concluded that physisorption is dominant in all the studied cases. The values of q_{DR}

411   range from 99.2 to 196.4 mg g^{-1}, depending on the observed material. These values

412   are of the order of others reported in the literature so far (Lazarević-Pašti et al., 2016).

413   Nevertheless, it should be noted that the DR model has lower values of

414   correlation coefficients (0.799 < R^2 < 0.84), so the exact values of adsorption

415   parameters should be taken with care. However, the conclusion regarding dominant

416   physisorption is valid, considering a good fit using Freundlich isotherm. Moreover,

417   q_{DR} values agree with experimentally derived adsorption capacities (Section 3.4),

418   noting that q_{DR} are maximum adsorption capacities, which were not reached in the

419   batch experiments for identical adsorbent concentrations.

420

Table 5. Summarized adsorption parameters for three adsorption isotherms used to fit experimental data. The sample DAHP-0.5 is emphasized as the one that shows the highest affinity towards dimethoate.

DAHP-X		Freundlich			Lagmuir			Dubinin-Radushkevich		
	n	K_f / mg g^{-1} (mg dm^{-3})$^{1/n}$	R^2	q_{max} /10^3 / mg g^{-1}	b / dm^3 mg^{-1}	R^2	q_{DR} / mg g^{-1}	K_{DR} /10^{-7} / mol^2 J^{-2}	E / kJ mol^{-1}	R^2
0	1.561	29.09	0.996	3.96	0.008	0.984	186.7	1.481	1.84	0.813
0.25	1.596	18.53	0.996	2.54	0.007	0.982	134.2	2.179	1.52	0.817
0.5	**1.661**	**35.82**	**0.994**	**4.71**	**0.010**	**0.989**	**196.4**	**1.104**	**2.13**	**0.823**
1	1.652	31.88	0.995	4.12	0.009	0.987	184.2	1.239	2.01	0.822
1.5	1.411	19.11	0.998	3.11	0.006	0.972	165.1	2.490	1.42	0.799
2	1.461	17.28	0.989	5.20	0.003	0.994	149.2	2.813	1.33	0.831
2.5	1.601	21.63	0.987	4.58	0.005	0.994	151.0	2.020	1.57	0.840
5	1.485	15.99	0.988	4.90	0.003	0.995	137.9	2.959	1.30	0.836
7.5	1.369	9.91	0.997	2.33	0.004	0.997	110.2	4.389	1.07	0.804
10	1.408	9.15	0.993	2.80	0.003	0.990	99.2	4.655	1.04	0.823

3.6. Materials properties and their link to dimethoate removal

Elucidating materials properties-performance relations is always a challenge, but it is utterly important to improve materials for given applications further. However, parametric space used to describe different materials in terms of their properties and performance can be huge, and it is essential to reduce it somehow. Even if this can be done only partially, making quantitative links between all these parameters can be rather useful for developing new materials. The approaches found in the literature differ by levels of complexity and sophistication, but here we would try to make it as simple as possible.

Presented ACFs were characterized by their chemical composition, textural properties, spectroscopic characteristics, and performance towards dimethoate removal. We chose simple multiple linear regression to link dimethoate removal

under different conditions (as dependent variable) with materials chemical composition (C, O, and P content) and textural properties (SSA and V_{tot}) as independent variables. The regression analysis results are summarized in **Table 6**, while parity plots are given in **Figure 9**.
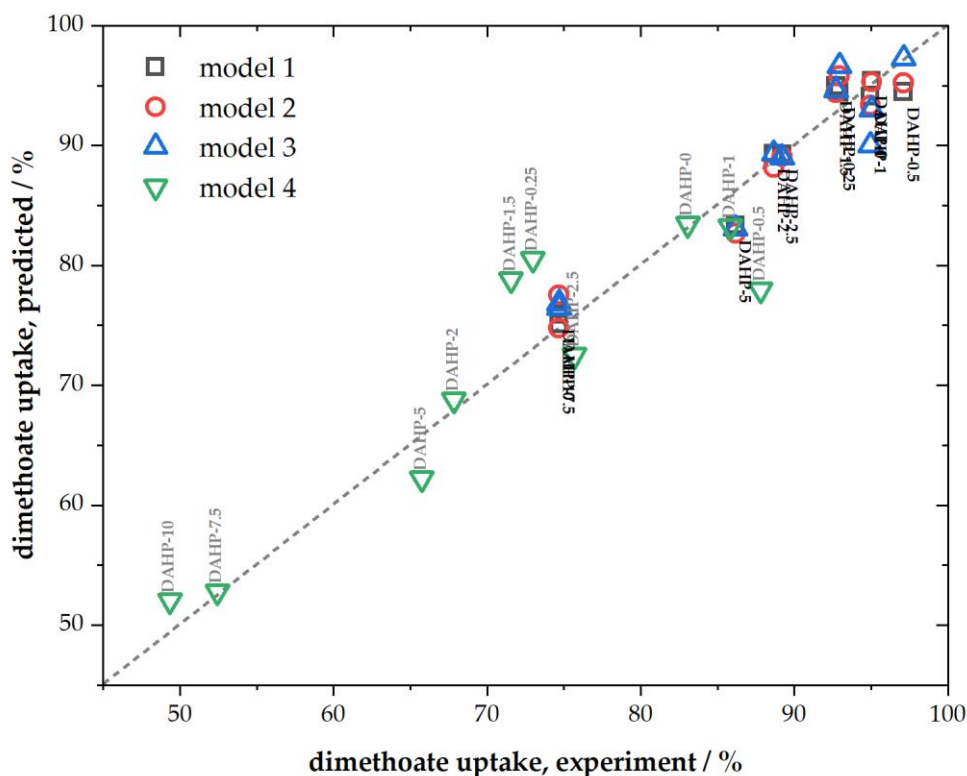
Table 6. The results of multiple linear regression analysis where dimethoate uptake (*UPT*) under different conditions is assumed to be connected to materials properties as UPT (%) = $A \times$ at.%(C) + $B \times$ at.%(O) + $C \times$ at.%(P) + $D \times$ SSA + $E \times V_{tot}$.

Conditions	*A*	*B*	*C*	*D* / % g m⁻²	*E* / % g cm⁻³	R^2	Model no.
1 mg cm⁻³ ACFs,	0.957	0.58	−6.1	0.006	−10.3	0.9994	1
5×10⁻⁴ mol dm⁻³	0.994	0.61	−7.1	/	−0.73	0.9992	2
dimethoate, batch	1.066	0.30	/	/	−8.5	0.998	3
0.1 mg cm⁻³ ACFs, 5×10⁻⁶ mol dm⁻³ dimethoate, batch	0.755	0.94	−18	0.005	−4.1	0.991	4

As can be seen, when all mentioned independent variables are taken into account, the fit is very good (R^2 = 0.9994, model no. 1, **Table 6**) for the conditions corresponding to a higher adsorbent and dimethoate concentration. The fit is slightly poorer for the conditions corresponding to lower concentrations of dimethoate and ACFs but still of rather high quality (model no. 4, **Table 6**). However, when it comes to rapid screening of materials as potential candidates for dimethoate removal, further reduction of the number of independent variables is desirable. As we have shown that SSA and V_{tot} mutually scale, one of these variables can be considered redundant (better scaling between them means that this approximation will work

455   better). Hence, when we remove SSA from the fit, we still get rather well predictions

456   of dimethoate uptake (model no. 2, **Table 6**). Further reduction is also possible

457   considering that P content scales with SSA and V_{tot}, and also that the sum of C, O,

458   and P content equals unity. In this case, using only three independent variables (C

459   and O content and V_{tot}), we, again, obtain very good linear regression with $R^2 = 0.998$

460   (model no. 3, **Table 6**). The possibility to exclude P content from the fit does not

461   mean that it is irrelevant – its presence tunes the total pore volume.

462   Moreover, it is very interesting that SSA does not have one of the leading

463   roles in the determination of dimethoate uptake (not only in regression analysis but

464   also in the batch and filtration experiments), particularly when having in mind that

465   high SSA ACFs also have larger pores (**Figure 4b**). However, with the increase of

466   SSA (and V_{tot}, Table 2) O content also increases (**Table 1**). This makes the surface

467   more hydrophilic and strongly solvated (hydrated). Considering that dimethoate is

468   physisorbed on studied ACFs surfaces and that its solubility in water is relatively

469   low, it is expected that weak dimethoate physisorption cannot compensate

470   (energetically) breaking of the solvation layer of ACFs. Hence, its uptake decreases

471   as the surface becomes more hydrophilic.

472

Figure 9. Parity plot for presented linear regression models

While connecting materials properties to dimethoate uptake can be done relatively easily using multiple linear regression, linking materials properties with synthesis conditions could be much more difficult. Therefore, it would likely require more sophisticated approaches like machine learning. However, if such relations are established, this would mean that one could set up a model for materials design for dimethoate removal with desired performance.

4. Conclusions

Series of ACFs was produced upon impregnation of viscose fibers with different amounts of DAHP. As the concentration of DAHP increased, O and P content, SSA, and V_{tot} were also found to increase. As a result, the SSA of studied

487   ACFs varied between 1000 and 2700 m^2 g^{-1}. These materials were studied as

488   adsorbents for dimethoate, and high dimethoate uptake was found for all materials,

489   even in dimethoate solutions with a concentration as high as 5×10^{-4} mol dm^{-3}.

490   Furthermore, the materials performed excellently in deionized water solutions and

491   spiked tap water samples, suggesting that matrix effects are minor, while the high

492   efficiency of dimethoate removal was also confirmed under dynamic (filtration)

493   experiments. The latter point, connected with the fact that toxicity of water samples

494   is significantly reduced upon the treatment, suggests that studied ACFs have a high

495   potential for implementation into the water purification systems. This relates

496   specifically to ACFs produced with low concentrations of DAHP as impregnation

497   agent, which performed the best as adsorbents for dimethoate and have the highest

498   production yield, which is very important for rationalizing the entire process, from

499   ACFs production to their use as adsorbents. We found that SSA is not the key factor

500   for efficient dimethoate uptake. Instead, we found simple linear regression

501   connecting C and O content, and total pore volume can be used to predict

502   dimethoate uptake in the studied series ACFs reliably. It is suggested that a balance

503   between pore size distribution, carbon content, and hydrophilicity of the ACFs

504   surface (linked to O content and directly influenced by the amount of incorporated

505   P) leads to the maximum performance in dimethoate removal from contaminated

506   water.

507

508   **Acknowledgment**

516

517 References

518 Ahmad, A.L., Tan, L.S., Shukor, S.R.A., 2008. Dimethoate and atrazine retention from
519   aqueous solution by nanofiltration membranes. J. Hazard. Mater. 151, 71–77.
520   https://doi.org/10.1016/j.jhazmat.2007.05.047

521 Al-ghouti, M.A., Da'ana, D., 2020. Guidelines for the use and interpretation of adsorption
522   isotherm models: A review. J. Hazard. Mater. 393, 122383.
523   https://doi.org/10.1016/j.jhazmat.2020.122383

524 Anićijević, V., Jelić, M., Jovanović, A., Potkonjak, N., Pašti, I., Lazarević-Pašti, T., 2021.
525   Organophosphorous pesticide removal from water by graphene-based materials – Only
526   adsorption or something else as well? J. Serbian Chem. Soc. 1–12.

527 Berber-Mendoza, M.S., Martínez-Costa, J.I., Leyva-Ramos, R., Amezquita Garcia, H.J.,
528   Medellín Castillo, N.A., 2018. Competitive Adsorption of Heavy Metals from Aqueous
529   Solution onto Oxidized Activated Carbon Fiber. Water. Air. Soil Pollut. 229.
530   https://doi.org/10.1007/s11270-018-3906-y

531 Breitenbach, S., Gavrilov, N., Pašti, I., Unterweger, C., Duchoslav, J., Stifter, D., Hassel, A.W.,
532   Fürst, C., 2021. Biomass-Derived Carbons as Versatile Materials for Energy-Related
533   Applications: Capacitive Properties vs. Oxygen Reduction Reaction Catalysis. C 7, 55.
534   https://doi.org/10.3390/c7030055

535 Breitenbach, S., Lumetzberger, A., Hobisch, M.A., Unterweger, C., Spirk, S., Stifter, D., Fürst,
536   C., Hassel, A.W., 2020. Supercapacitor Electrodes from Viscose-Based Activated Carbon
537   Fibers: Significant Yield and Performance Improvement Using Diammonium Hydrogen
538   Phosphate as Impregnating Agent. C — J. Carbon Res. 6, 17.
539   https://doi.org/10.3390/c6020017

540 Chen, J.Q., Wang, D., Zhu, M.X., Gao, C.J., 2007. Photocatalytic degradation of dimethoate
541   using nanosized TiO2 powder. Desalination 207, 87–94.
542   https://doi.org/10.1016/j.desal.2006.06.012

543 Chishti, Z., Hussain, S., Arshad, K.R., Khalid, A., Arshad, M., 2013. Microbial degradation of
544   chlorpyrifos in liquid media and soil. J. Environ. Manage. 114, 372–380.

545 https://doi.org/10.1016/j.jenvman.2012.10.032

546 Colovic, M.B., Krstic, D.Z., Lazarevic-Pasti, T.D., Bondzic, A.M., Vasic, V.M., 2013.
547 Acetylcholinesterase Inhibitors: Pharmacology and Toxicology. Curr. Neuropharmacol.
548 11, 315–335. https://doi.org/10.2174/1570159x11311030006

549 Cougnaud, A., Faur, C., Le Cloirec, P., 2005. Removal of pesticides from aqueous solution:
550 Quantitative relationship between activated carbon characteristics and adsorption
551 properties. Environ. Technol. 26, 857–866. https://doi.org/10.1080/09593332608618497

552 Ellman, G.L., Courtney, K.D., Andres, V., Featherstone, R.M., 1961. A new and rapid
553 colorimetric determination of acetylcholinesterase activity. Biochem. Pharmacol. 7, 88–
554 95. https://doi.org/https://doi.org/10.1016/0006-2952(61)90145-9

555 Farner Budarz, J., Cooper, E.M., Gardner, C., Hodzic, E., Ferguson, P.L., Gunsch, C.K.,
556 Wiesner, M.R., 2019. Chlorpyrifos degradation via photoreactive TiO2 nanoparticles:
557 Assessing the impact of a multi-component degradation scenario. J. Hazard. Mater. 372,
558 61–68. https://doi.org/10.1016/j.jhazmat.2017.12.028

559 Faur, C., Métivier-Pignon, H., Le Cloirec, P., 2005. Multicomponent adsorption of pesticides
560 onto activated carbon fibers. Adsorption 11, 479–490. https://doi.org/10.1007/s10450-
561 005-5607-2

562 Ferrari, A.C., Robertson, J., 2000. Interpretation of Raman spectra of disordered and
563 amorphous carbon. Phys. Rev. B 61, 14095. https://doi.org/10.1007/BF02543692

564 Hassan, M.F., Sabri, M.A., Fazal, H., Hafeez, A., Shezad, N., Hussain, M., 2020. Recent trends
565 in activated carbon fibers production from various precursors and applications—A
566 comparative review. J. Anal. Appl. Pyrolysis 145, 104715.
567 https://doi.org/10.1016/j.jaap.2019.104715

568 Ishag, A.E.S.A., Abdelbagi, A.O., Hammad, A.M.A., Elsheikh, E.A.E., Elsaid, O.E., Hur, J.H.,
569 Laing, M.D., 2016. Biodegradation of Chlorpyrifos, Malathion, and Dimethoate by
570 Three Strains of Bacteria Isolated from Pesticide-Polluted Soils in Sudan. J. Agric. Food
571 Chem. 64, 8491–8498. https://doi.org/10.1021/acs.jafc.6b03334

572 Jacob, M.M., Ponnuchamy, M., Kapoor, A., Sivaraman, P., 2020. Bagasse based biochar for
573 the adsorptive removal of chlorpyrifos from contaminated water. J. Environ. Chem.
574 Eng. 8, 103904. https://doi.org/10.1016/j.jece.2020.103904

575 Lazarević-Pašti, T.D., Pašti, I.A., Jokić, B., Babić, B.M., Vasić, V.M., 2016. Heteroatom-doped
576 mesoporous carbons as efficient adsorbents for removal of dimethoate and omethoate
577 from water. RSC Adv. 6, 62128–62139. https://doi.org/10.1039/c6ra06736k

578 Liu, G., Li, L., Huang, X., Zheng, S., Xu, X., Liu, Z., Zhang, Y., Wang, J., Lin, H., Xu, D., 2018.
579 Adsorption and removal of organophosphorus pesticides from environmental water
580 and soil samples by using magnetic multi-walled carbon nanotubes @ organic
581 framework ZIF-8. J. Mater. Sci. 53, 10772–10783. https://doi.org/10.1007/s10853-018-
582 2352-y

583 Martin-Gullon, I., Font, R., 2001. Dynamic pesticide removal with activated carbon fibers.
584 Water Res. 35, 516–520. https://doi.org/10.1016/S0043-1354(00)00262-1

585 Mojiri, A., Zhou, J.L., Robinson, B., Ohashi, A., Ozaki, N., Kindaichi, T., Farraji, H., Vakili,
586 M., 2020. Pesticides in aquatic environments and their removal by adsorption methods.
587 Chemosphere 253, 126646. https://doi.org/10.1016/j.chemosphere.2020.126646

588 Momić, T., Pašti, T.L., Bogdanović, U., Vodnik, V., Mraković, A., Rakočević, Z., Pavlović,
589   V.B., Vasić, V., 2016. Adsorption of Organophosphate Pesticide Dimethoate on Gold
590   Nanospheres   and   Nanorods.   J.   Nanomater.   2016.
591   https://doi.org/10.1155/2016/8910271

592 Samy, M., Ibrahim, M.G., Gar Alalm, M., Fujii, M., Diab, K.E., ElKady, M., 2020. Innovative
593   photocatalytic reactor for the degradation of chlorpyrifos using a coated composite of
594   ZrV2O7   and   graphene   nano-platelets.   Chem.   Eng.   J.   395,   124974.
595   https://doi.org/10.1016/j.cej.2020.124974

596 Shanmuga Priya, M., Divya, P., Rajalakshmi, R., 2020. A review status on characterization
597   and electrochemical behaviour of biomass derived carbon materials for energy storage
598   supercapacitors.   Sustain.   Chem.   Pharm.   16,   100243.
599   https://doi.org/10.1016/j.scp.2020.100243

600 Shimodaira, N., Masui, A., 2002. Raman spectroscopic investigations of activated carbon
601   materials. J. Appl. Phys. 92, 902–909. https://doi.org/10.1063/1.1487434

602 Thomas, L.C., Chittenden, R.A., 1965. Characteristic infra-red absorption frequencies of
603   organophosphorus compounds—V: Phosphorus—carbon bonds 21, 1905–1914.

604 Tian, F., Liu, W., Guo, G., Qiang, Z., Zhang, C., 2014. Chemosphere Kinetics and mechanism
605   of dimethoate chlorination during drinking water treatment. Chemosphere 103, 181–
606   187. https://doi.org/10.1016/j.chemosphere.2013.11.061

607 Țucureanu, V., Matei, A., Avram, A.M., 2016. FTIR Spectroscopy for Carbon Family Study.
608   Crit. Rev. Anal. Chem. 46, 502–520. https://doi.org/10.1080/10408347.2016.1157013

609 Wanjeri, V.W.O., Sheppard, C.J., Prinsloo, A.R.E., Ngila, J.C., Ndungu, P.G., 2018. Isotherm
610   and kinetic investigations on the adsorption of organophosphorus pesticides on
611   graphene oxide based silica coated magnetic nanoparticles functionalized with 2-
612   phenylethylamine.   J.   Environ.   Chem.   Eng.   6,   1333–1346.
613   https://doi.org/10.1016/j.jece.2018.01.064

614 WHO, 2020. The WHO Recommended Classification of Pesticides by Hazard and Guidelines
615   to Classification.

616 WHO, 2017. Guidelines for Drinking-water Quality. WHO Library Cataloguing-in-
617   Publication Data.

618 Zhao, Y., Cho, C.W., Wang, D., Choi, J.W., Lin, S., Yun, Y.S., 2020. Simultaneous scavenging
619   of persistent pharmaceuticals with different charges by activated carbon fiber from
620   aqueous   environments.   Chemosphere   247,   125909.
621   https://doi.org/10.1016/j.chemosphere.2020.125909

622